PAPER

Limits on the use of cobalt sulfide as anode of p-type dye-sensitized solar cells

To cite this article: Matteo Bonomo *et al* 2017 *J. Phys. D: Appl. Phys.* **50** 215501

View the article online for updates and enhancements.

Related content

- Monolithic quantum dot sensitized solar cells
  M Samadpour, Z Ghane, N Ghazyani et al.

- Enhanced performance of dye-sensitized solar cells using gold nanoparticles modified fluorine tin oxide electrodes
  Dingwen Zhang, Milton Wang, Alexandre G Brolo et al.

- Electrodeposited ZnO with squaraine sentisizers as photoactive anode of DSCs
  Iole Venditti, Nadia Barbero, Maria Vittoria Russo et al.

Recent citations

- New pyran-based dyes as efficient sensitizers of p -type dye-sensitized solar cells
  Matteo Bonomo *et al*

- Structural, electrical and photovoltaic properties of CoS/Si heterojunction prepared by spray pyrolysis
  I M El Radaf *et al*

IOP e**books**™

Bringing you innovative digital publishing with leading voices to create your essential collection of books in STEM research.

Start exploring the collection - download the first chapter of every title for free.

Limits on the use of cobalt sulfide as anode of p-type dye-sensitized solar cells*

Matteo Bonomo[1,6]**, Mirko Congiu**[2]**, Maria Letizia De Marco**[1]**,
Denis P Dowling**[3]**, Aldo Di Carlo**[4]**, Carlos F O Graeff**[2,5] **and Danilo Dini**[1,6]

[1] Department of Chemistry, University of Rome 'La Sapienza', Piazzale Aldo Moro 5, Rome, RM, Italy

[2] UNESP—Universidade Estadual Paulista, POSMAT—Programa de Pós-Graduação em Ciência e Tecnologia de Materiais, Av. Eng. Luiz Edmundo Carrijo Coube14-01, 17033-360 Bauru, SP, Brazil

[3] University College Dublin, UCD, Belfield, Dublin 4, Ireland

[4] Department of Electrical Engineering, C.H.O.S.E.-Center for hybrid and organic solar energy, University of Roma 'Tor Vergata', via del Politecnico 1, 00133, Rome, Italy

[5] DC-FC—UNESP—Universidade Estadual Paulista, Av. Eng. Luiz Edmundo Carrijo Coube14-01, 17033-360 Bauru, SP, Brazil

E-mail: danilo.dini@uniroma1.it and matteo.bonomo@uniroma1.it

Abstract

Thin films of cobalt sulfide (CoS) of thickness $l < 10$ μm have been employed as anodes of p-type dye-sensitized solar cells (p-DSCs) when P1-sensitized nickel oxide (NiO) was the photoactive cathode and I_3^-/I^- constituted the redox mediator. In the role of counter electrode for p-DSCs, CoS was preferred over traditional platinized fluorine-doped indium oxide (Pt-FTO) due to the lower cost of the starting materials (Co salts) and the easier procedure of deposition onto large area substrates. The latter process was carried out via direct precipitation of CoS from aqueous solutions. The photoconversion efficiency (η) of the corresponding device was 0.07%. This value is about 35% less than the efficiency that is obtained with the analogous p-DSC employing the Pt-FTO anode ($\eta = 0.11$). Unlike p-DSCs based on Pt-FTO anodes, the photoelectrochemical cells employing CoS electrodes showed that this anodic material was not able to sustain the photocurrent densities generated by P1-sensitized NiO at a given photopotential. Illumination of the p-DSCs with CoS anodes and P1-sensitized NiO cathodes actually induced the reverse bias of the photoelectrochemical cell with CoS behaving like a p-type semiconductor with no degeneracy.

Keywords: dye-sensitized solar cell, CoS, NiO, semiconductor electrochemistry, photocathodes, DSC

S Supplementary material for this article is available online

(Some figures may appear in colour only in the online journal)

Introduction

Among the devices for solar radiation conversion, dye-sensitized solar cells (DSCs) [1] play an important role because of their high efficiencies (about 15%) [2–5], low costs of production, and employment in energy efficient fenestration due to the partial optical transparency of a DSC [6]. These photoelectrochemical cells can be divided into two categories: n- and p-type if oxidation and reduction are the electrochemical processes respectively activated by light absoprtion [7, 8]. The n-DSCs display a comparatively better performance than the p-type analogues since n-DSCs reach efficiencies of about 14% [3] whereas p-DSCs [9–11] present values still below 2% [12–14]. To reduce of the gap between n- and p-type DSC performances researchers are pursuing the preparation of photoactive cathodes affording larger photocurrent densities via the preparation of electrodic materials with increasing surface area [15–20] and new dye-sensitizers

---

[6] Author to whom any correspondence should be addressed.
* Dedicated to Professor Roberto Federici on the occasion of his retirement.

appositely designed for *p*-DSCs cathodes [19]. Besides the aspect of the improvement of the *p*-DSC performance, another important issue is of an economic nature and concerns the abatement of the costs of the materials employed in the *p*-DSC. In general, the most expensive element of a DSC is represented by the counter-electrode of platinized fluorine-doped tin oxide (Pt-FTO), i.e. the non-photoactive electrode, for which several low-cost alternatives have been proposed [21–30]. In a previous work we have demonstrated the feasibility of CoS as a low-cost alternative anode in a *p*-DSC with NiO photocathode and erythrosine B as dye-sensitizer [31]. In that work we showed that the replacement of Pt-FTO with CoS as the anodic material of a *p*-DSC did not bring about a considerable diminution of its overall efficiency (0.026 versus 0.030% for the photoelectrochemical cell with CoS and Pt-FTO, respectively) despite the *p*-type nature of CoS and its hole-collector properties [32–39]. For this reason, we have continued here our study on *p*-DSCs with CoS anodes and P1-sensitized NiO photocathodes [21, 23]. P1 is a dye known for having a stronger sensitizing action on NiO with respect to erythrosine B by virtue of the favourable electronic properties imparted by the triarylamine unit in P1 [40–44]. The content of the present paper is the analysis of the photoelectrochemical performance of the *p*-DSCs assembled with P1-sensitized NiO photocathodes [21, 23] when the anodes are made of *p*-type CoS thin films ($l < 10$ μm). This study is conducted for the first time with the purpose of determining the actual capability of low-cost CoS counter electrodes to sustain the larger photocurrent densities of P1-sensitized *p*-DSCs with respect to erythrosine B-sensitized *p*-DSCs. For comparative purposes we have also analysed the photoelectrochemical behaviour of the *p*-DSCs employing Pt-FTO counter electrodes in analogous experimental conditions.

Experimental section

Cobalt chloride hexahydrate (CoCl$_2$·6H$_2$O), thioglycolic acid (TGA), ethanol (EtOH), methanol (MeOH), acetonitrile (ACN), fluorine-doped tin oxide coated glass slides (FTO) with sheet resistance (~7 Ω cm^{-2}), and NiO nanoparticles (99.8% grade with average diameter ~50 nm), were purchased from Sigma-Aldrich. All these reagents were used without any further purification. Dye-sensitizer P1 was purchased from Dyenamo (Sweden). Platisol T\SP paste and high stability I^-/I_3^- electrolyte (HSE) of the type BV12 were purchased from Dyers (Italy) and Solaronix (Switzerland), respectively. The UV-resin 3035 B was purchased from Threebond and was used as the sealing and separating agent. The thickness of the NiO film was 2 μm as estimated with a scanning profilometer [19]. Electrode surface roughness was estimated with a Wyko NT1100 optical profilometer in the vertical scanning interferometry mode (VSI). X-ray characterization of the working electrodes was carried out using a Siemens D500 diffractometer with the Cu kα radiation at the scan rate of 0.2° min^{-1}. The crystallite size of the mesoporous NiO films was calculated by Gaussian fit of the peaks using the Scherrer equation. Counter-electrodes and FTO transmittance measurements were made using a double ray spectrometer (UV-2550 by Shimazdu). The photovoltaic

performance of the cells was evaluated using a solar simulator Solar Test 1200 KHS (class B) with 1000 W m^{-2} (AM 1.5 G) as the light source. Incident photon-to-current conversion efficiency (IPCE) spectra were recorded using a computer controlled setup consisting of a Xe lamp (Mod.70 612, Newport) coupled to a monochromator (Cornerstone 130, from Newport), and a Keithley 2420 light source meter. Cyclic voltammetries were conducted with an AUTOLAB PGSTAT12® (Metrohm) in the potential range $-1 \leqslant E \leqslant +1$ V versus Ag/AgCl reference electrode. The determination of the electrochemical impedance spectra (EIS) of the two electrode cells was performed with AUTOLAB PGSTAT12® (Metrohm) under the conditions of open circuit potential. The EIS profiles of the assembled *p*-DSCs were recorded in dark conditions and under illumination with the light source specified above. For the symmetrical cells with CoS as sole electrodic material, and Pt as sole electrodic material, the EIS profiles were recorded in the dark at the polarization of 0 V (short circuit condition). For EIS experiments the sinusoidal perturbation of the potential had an amplitude of 10^{-2} V and it was applied within the frequency range 10^{-1}–10^5 Hz for the measurements under illumination and for the symmetrical two electrode cells employing a single electrodic material. The frequency range 10^{-2}–10^5 Hz was considered for the dark measurements of the DSCs. Measurements with light-soaked cells were carried out with a solar simulator Solar Test 1200 KHS (class B) at 1000 W m^{-2} (AM 1.5 G). In order to calculate the electrochemical cells parameters derived from the analysis of the EIS profiles, the impedance spectra were fitted using the software Z-View 2.1. All graphs were realized with Kaleidagraph 3.6 software. Details of the preparation of CoS-FTO and Pt-FTO counter electrodes, and the description of the deposition technique for the NiO samples here employed have been reported in previous works [31, 45]. NiO films were sensitized with P1 by dipping the electrode in a 0.3 mM dye solution in ACN for 16 hours. The NiO electrode sensitization was carried out in dark conditions to prevent possible photo-oxidation of the sensitizer in the solution of sensitization. The photocathode was successively rinsed with pure ACN to remove the molecules of dye that did not get chemisorbed onto NiO. Successively, the sensitized working electrode was sealed to the counter electrode using a Bynel® thermoplastic spacer. After sealing the electrolyte HSE (from Dyesol) was injected by vacuum back-filling, using a little hole in the polymer mask. Upon completion of the filling step, the cell was closed using a UV-cured thermoplastic resin. The details on the characterization of CoS films have been reported in a previous paper [31].

Results and discussion

General characterization of CoS film

Figure 1 reports a comparison of the optical transmission spectra of CoS and Pt-FTO anodes in the visible range when these electrodes are in the configuration of thin film as in the real device.
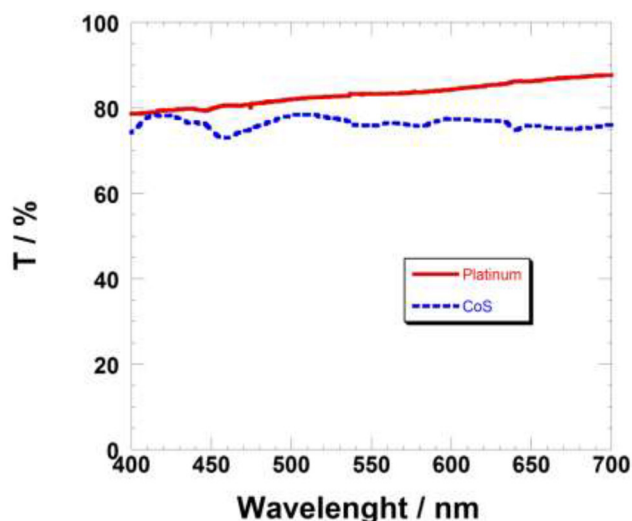
J. Phys. D: Appl. Phys. **50** (2017) 215501

M Bonomo *et al*

Figure 1. Transmittance spectra of CoS (blue trace) and Pt-FTO (red trace) thin films prior to their assembly in the respective *p*-DSCs. These profiles have been determined utilizing bare FTO in air as blank.

In figure 1 the film of Pt-FTO presents a high optical transmission with a quasi-uniform profile when the radiation falls in the wavelength range 400–700 nm. In the same spectral range the optical transmission of CoS presents an undulating profile with an average transmittance of 75%. In the present case thin films of CoS represent a poorly absorbing material in the wavelength range 400–700 nm. Under such circumstances, it is customary to attribute the origin of such wavy features to the fringes of interference when the film has a thickness of the same order of magnitude as the radiation wavelength or a multiple of it [46]. It is known from the literature that cobalt sulfides possess a featureless absorption spectrum at wavelengths larger than 350 nm [47]. Therefore, the wavy profile for the optical transmission spectrum of CoS combined with the quite large average transmittance of CoS film (≈75%, figure 1) indicates that the system under examination is optically a thin film.

It has also been observed that CoS does not cover uniformly the FTO substrate as evidenced by SEM investigation (see supplemental information (stacks.iop.org/JPhysD/50/215501/mmedia)). The presence of cracks in the CoS films as well as the presence of zones of uncovered substrate further diminish the contribution of CoS to the optical absorption of the whole system.

In the wavelength range 550–700 nm, CoS was about 10% less transparent than Pt-FTO, whereas the two different counter electrodes present analogous transmittance in the range 400–550 nm. Given these absorption characteristics of the counter electrodes, the incident radiation should then allow the excitation of the sensitized photocathode at the same extent when illumination is projected first on the back side of the *p*-DSC where the anode stands [48].

The voltammograms of CoS and Pt-FTO in a non-aqueous electrolyte containing the redox couple I^-/I_3^- (figure 2, plot A) indicate that both electrodes are polarizable and, as such, present quasi-metallic features. Neither CoS nor Pt-FTO

electrodes underwent redox processes within the potential range in which the redox couple I^-/I_3^- operates as shuttle in a *p*-DSC [49].

The slopes of the voltammograms of CoS and Pt-FTO in the linear regime (figure 2, plot (A)) are directly proportional to the charge transfer resistance of the electrodes towards the redox processes based on the I^-/I_3^- couple. Therefore, the similarity of these slopes indicates similar electrical resistance for the two different counter electrodes. At the end of the linear portion of the voltammogram, the current profile becomes horizontal with the current reaching a limiting value of *plateau*. The height of the *plateau* has a module which depends on the concentration of the redox active species in the electrolyte, and on their diffusion coefficients [50]. The values of the limiting current were 13.47 and 13.87 mA cm^{-2} for Pt-FTO and CoS, respectively. The EIS of the symmetric cells having the two electrodes of the same material (figure 2, plot (B)) have been interpolated with the Randles model [51] (see inset in plot (B) of figure 2). The circuital elements that characterize the electrochemical behaviour of the electrode are the charge transfer resistance through the electrode/electrolyte interface (R_{ct}), and the capacitance (C_{dl}) associated with the charge separation of the double layer at the electrode/electrolyte interface. In the equivalent circuit of figure 2 (plot (B)) the resistive term R_s represents the series resistance of the electrolyte in series with the resistance of the external circuit and other various linear ohmic elements of the two-electrode cell. The model of the equivalent circuit also includes the Warburg element W_s in series with R_{ct}, with W_s describing the intrinsic transport properties of the electrode itself under the given conditions of polarization. The fitting values of R_{ct} for CoS and Pt-FTO were 1.51 ± 0.08 and 2.30 ± 0.12 Ω cm^2, respectively. The lower value of R_{ct} for CoS evidences a higher electrocatalytic activity of CoS with respect to platinized FTO towards the redox reactions involving the redox shuttle I^-/I_3^- in dark conditions. The double layer capacitance C_{dl} was 13.01 ± 0.87 and 40.09 ± 1.32 μF cm^{-2} for CoS and Pt-FTO, respectively. Such a difference shows how Pt-FTO retains a greater amount of surface charge with respect to CoS. The second semicircle of the impedance spectra at lower frequencies, i.e. the semicircle on the right portion of the impedance spectra, is associated with the diffusion of the redox species in the electrolyte and will not be further discussed since it does not depend on the intrinsic characteristics of the anode.

Analysis of p-DSCs with CoS anode

The *JV* characteristic curves of the two *p*-DSCs differing for the nature of the anode are shown in figure 3.

The relative parameters of the photoelectrochemical cells of figure 3 have been listed in table 1.

The values of open circuit potential (V_{OC}) are not affected by the nature of the anode being the difference of V_{OC} within the experimental error. This reveals the metallic behavior of the two different counter electrodes here considered under the condition of open circuit. In fact, V_{OC} is determined exclusively by the difference between the Nernst potential of the

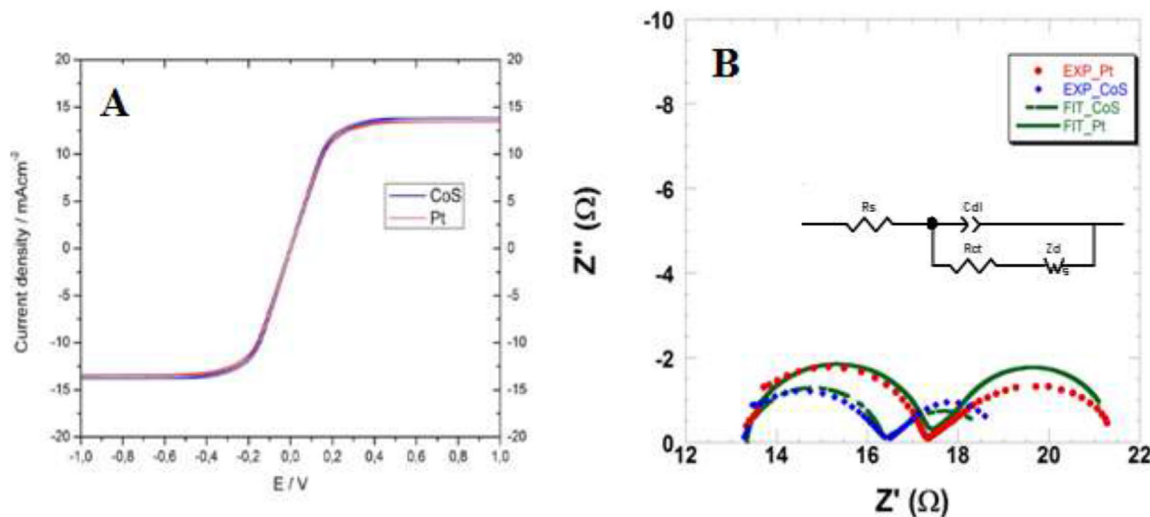J. Phys. D: Appl. Phys. **50** (2017) 215501

M Bonomo *et al*

Figure 2. (A) Voltammograms of CoS (blue trace) and Pt-FTO (red trace) in the two-electrode symmetric cells with equal working and counter electrodes. (B) Corresponding EIS of the dummy cells of the left frame at null potential. Blue and red empty circles refer to CoS and Pt-FTO spectral profiles, respectively. The two green lines represent the fitting curves obtained with the equivalent Randles circuit in the inset. Both cyclic voltammetries (plot (A)) and EIS profiles (plot (B)) were carried out in dark conditions. The iodine-based electrolyte was BV12-HSE.
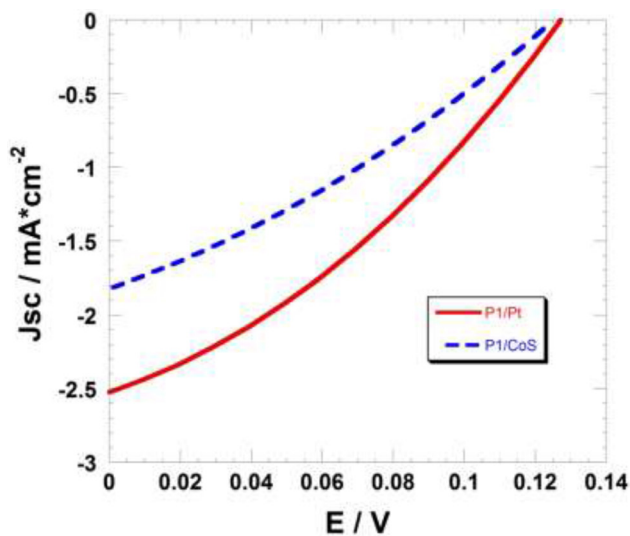

Figure 3. *JV* characteristic curves of the *p*-DSCs employing CoS (blue) or Pt-FTO (red) as anode. The photoactive cathode was P1-sensitized NiO. Photocurrent density profiles were recorded when the cells were illuminated from the front side, i.e. with the light first incident on the cathode.

redox couple and the upper edge of the valence band of illuminated NiO when the oxide is in the sensitized state [52]. On the other hand, the most important differences have been found for the overall efficiencies values and the cathodic short circuit current density values for the two *p*-DSCs differing for the anode (table 1). The values of η and J_{SC} were respectively 0.11% and -2.45 mA cm^{-2} for the device with the Pt-FTO anode, and 0.07% and -1.70 mA cm^{-2} for the *p*-DSC with CoS as counter electrode. The value of the FF was approximately the same for the two cells, differing for the anode (*ca*. 32%, table 1).

In terms of external quantum efficiency, the curves of the IPCE have a shape which does not change with the nature

of the anodic material (figure 4). This finding is expectable since both anodes are poorly absorbing materials in the visible spectrum (figure 1, see above). The generally lower spectral efficiency of the CoS based *p*-DSC with respect to the *p*-DSC with the Pt-FTO anode is consistent with the trend of the short circuit current density (table 1).

For the evaluation of the charge transport characteristics of the two different anodes, we considered the technique of photoelectrochemical impedance spectroscopy [53]. This consists of the recording of the EIS of the *p*-DSCs under illumination at the potential of open circuit. For both types of *p*-DSCs, we selected the most performing photoelectrochemical cell within the set of three cells assembled per type of *p*-DSC. The experimental spectra and the fitting curves are reported in figure 5 for the two different *p*-DSCs.

The high-frequencies semicircle in the lower left end of the spectrum is associated with the kinetics of the charge-transfer processes at the anode of the *p*-DSC [54]. The larger the diameter of this semicircle, the larger the charge-transfer resistance through the anode/electrolyte interface. The electrochemical process in question is the oxidation of iodide to tri-iodide at the anodes of CoS and Pt-FTO. In general, the overall efficiency of the photoelectrochemical cell diminishes upon the increase of the charge transfer resistance at the anode. This is because a larger charge transfer resistance at the anode/electrolyte interface will correspond to a slower kinetics of iodide oxidation. The anode of CoS presents a larger charge transfer resistance with respect to Pt-FTO in the corresponding *p*-DSC (figure 5). Because of this difference, CoS will regenerate the oxidized form of the redox shuttle at a lower rate in comparison to Pt/FTO. This difference of charge transfer kinetics between CoS and Pt-FTO is more evident when the photocurrent densities to sustain are relatively large ($J_{SC} > 2$ mA cm^{-2}) as in the case of P1-sensitized *p*-DSCs [20, 48]. In the case of *p*-DSCs employing a sensitizer less efficacious of P1, e.g. erythrosine

Table 1. Photovoltaic parameters obtained from the *JV* curves recorded when the potential was scanned from the short circuit value to 0.13 V under sun simulator with AM 1.5. Open circuit voltage (V_{OC}), short circuit current (J_{SC}), fill factor (FF) and overall energy conversion efficiency (η) are reported. The value of IPCE (incident photon-to-current conversion efficiency) refers to the wavelength of maximum absorption of the P1 colorant ($\lambda_{MAX} = 475$ nm). The errors are determined by the dispersion of the values registered during the analysis of three nominally equal devices.

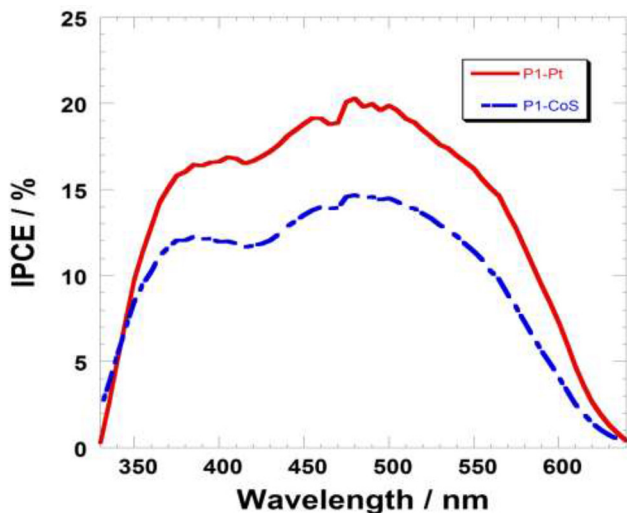| *p*-DSC anode	V_{OC} / mV	J_{SC} / mA cm^{-2}	FF / %	η / %	IPCE / %
Pt-FTO	129 ± 1	−2.45 ± 0.12	32.7 ± 1.2	0.108 ± 0.01	20.2 ± 0.1
CoS-FTO	128 ± 1	−1.70 ± 0.08	31.7 ± 1.3	0.070 ± 0.08	14.6 ± 0.1

Figure 4. IPCE spectra of the *p*-DSCs with Pt-FTO (red) and CoS (blue) anodes when P1-sensitized NiO is the photoactive cathode.
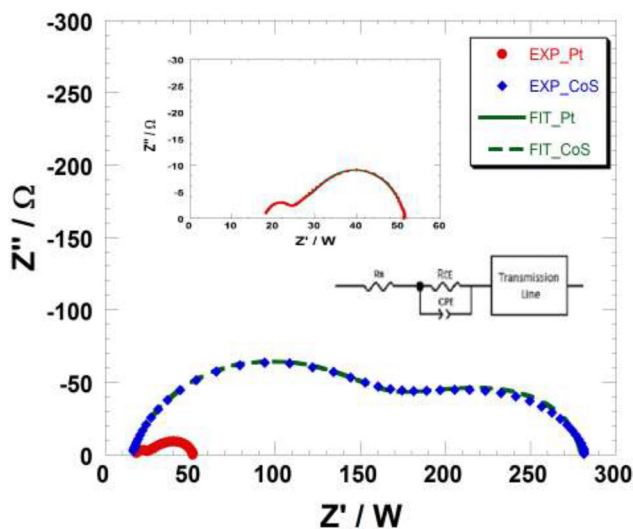

Figure 5. Photoelectrochemical impedance spectra of the *p*-DSCs differing for the anode. The cell was polarized at the value of V_{OC} which was determined when the cell was soaked with 1 sun of illumination (table 1). The red circles refer to the impedance profile of the *p*-DSC with Pt-FTO anode. Blue diamonds indicate experimental data of the cell with CoS anode. Green lines indicate the fitting curves (full line for the Pt-FTO based *p*-DSC, dotted line for the CoS based *p*-DSC). The inset in the lower right end represents the equivalent circuit used to fit the experimental data of impedance for the complete *p*-DSC.

B [31], the charge transfer kinetics at the two different anodes is hardly distinguishable if the sole parameter of the overall efficiency is analysed. CoS anodes present a slightly larger

resistance of charge transfer (R_{ct}) with respect to Pt-FTO anodes when the *p*-DSC employs erythrosine B [31]. As previously stated, such differences of R_{ct} between CoS and Pt-FTO anodes are not sufficiently large to produce considerably different photocurrent densities and overall efficiencies in the respective *p*-DSCs [11, 55–60]. This set of findings leads us to conclude that CoS and Pt-FTO anodes perform in a practically equivalent manner when the photocurrent densities to sustain do not exceed the threshold of 2 mA cm^{-2}. We quantify such a threshold in the value of 2 mA cm^{-2}, i.e. the value corresponding to the maximum J_{SC} so far expressed by the CoS electrodes prepared with the method here considered [31]. In this regard, CoS anodes may represent a suitable cost-effective alternative to Pt-FTO counter electrodes provided that the photoelectrochemical devices do not operate in high-performing conditions. For a wider employment of CoS films as the anode of a *p*-DSC some requirements need to be fulfilled. First of all, the deposition of a less defective film of CoS (possibly with a non-amorphous structure—see XRD data in supplemental material): this would allow a better definition of the electronic surface states that are responsible for the oxidative processes. Second, the preparation of a nanostructured film of CoS: the existence of a nanostructure with a high surface area would bring about the increase of surface density of the electrochemically active sites for the oxidation process. From the realization of these two points an enhancement of the kinetics of oxidation at the CoS anode is expected. As a consequence of that, also the overall efficiency of the device would be increased.

The photoelectrochemical impedance spectra of the *p*-DSCs under illumination at the open circuit photopotential (figure 5) have been fitted with the equivalent circuit depicted in the inset of figure 5. The circuital elements R_{CE} and CPE (constant phase element) refer to the electrical characteristics of the counter electrode made of CoS or Pt-FTO. These circuital elements are combined in parallel and represent respectively the nonlinear resistance of charge transfer through the anode/electrolyte interface, and the capacitive element related to the charge distribution and charge separation at the anode/electrolyte interface [61]. The transmission line of the equivalent circuit in the inset of figure 5 constitutes the model that better describes the electrical properties of a dye-sensitized nanostructured semiconductor with localized electronic states [61]. Table 2 reports the values of charge transfer resistance R_{CE} at the anode/electrolyte interface for the two different counter electrodes, and the values of capacitance C_{CE} at the anode/electrolyte interface. The CoS electrode presents an interfacial resistance value that is about 30 times larger than the corresponding parameter of Pt-FTO (4.4 versus 130 Ω,

J. Phys. D: Appl. Phys. **50** (2017) 215501

M Bonomo *et al*

Table 2. Parameters of the *p*-DSCs associated with the electrical characteristics of Pt-FTO and CoS anodes. The values of R_{CE} and C_{CE} were obtained by fitting the experimental spectrum with the equivalent circuit of the inset in figure 5.

Anode	R_{CE} / Ω	$C_{CE} / \mu F$
Pt-FTO	4.4 ± 0.1	2.85 ± 0.24
CoS-FTO	129.9 ± 2.6	1.39 ± 0.08

Table 3. Electrical (R_t, R_{rec}) and microscopic (L_h, D_h) parameters for P1-sensitized NiO when this constitutes the photocathode of the *p*-DSC and Pt-FTO is the counter-electrode. The impedance spectrum of the Pt-FTO based *p*-DSC (red dots in figure 5) has been fitted with the electrical parameters here listed. For the fit the equivalent circuit in the inset of figure 5 has been adapted. The microscopic terms L_h and D_h are related to the characteristics of the photogenerated charge carriers and have been derived from equations (1) and (2) [54].

R_t / Ω	R_{rec} / Ω	$L_h / \mu m$	$D_h / 10^{-6} \, cm^2 * s^{-1}$
10.7 ± 0.3	45.2 ± 0.5	4.1 ± 0.1	109.2 ± 3.3

table 2) whereas the capacitive term is of the same order of magnitude for both types of cells (in the order of a few micro-farad). This indicates that there are no system-specific inter-actions, like preferential adsorption or corrosive phenomena, between the anode and the electrolyte. Therefore, we reason-ably ascribe the poorer performance of the *p*-DSC with the CoS anode to the less efficient kinetics of charge transfer at the CoS anode with respect to Pt-FTO when the charge transfer process consists of the oxidation of iodide. This affirmation retains its validity when *p*-DSC photocurrents are relatively high as in the case of the *p*-DSCs with P1-sensitized NiO photocathodes.

The electrical parameters associated with the charge trans-port properties of the P1-sensitized NiO photocathode and to the charge distribution at the P1-sensitized NiO/electrolyte interface have been determined exclusively for the *p*-DSC with the best performing anode Pt-FTO. This is because the values of NiO transport resistance (R_t) and resistance of recombina-tion at the NiO/electrolyte interface (R_{rec}) are intrinsic of the electrochemical behavior of NiO and are not influenced by the electrical/electrochemical quality of the anode. Besides the electrical resistance of charge transport through the NiO film (R_t), and the resistance of iodide recombination with the photogenerated holes at the NiO surface (R_{rec}), we were also able to extract the microscopic properties of diffusion coef-ficient D_h (equation (1)) and diffusion length L_h (equation (2)) for the holes photoinjected in P1-sensitized NiO (table 3) according to the theoretical treatment reported in [35, 36] when Pt-FTO was the anode.

$$D_h = L_h^2/(R_t * C_\mu) \qquad (1)$$

$$L_h = l_*(R_{rec}/R_t)^{1/2}. \qquad (2)$$

In equation (1) C_μ represents the chemical capacitance associ-ated with the capability of a system to accept or release addi-tional electronic carriers upon variation of chemical potential.

The latter parameter changes during the process of charge carrier photoinjection following the optical excitation of the dye-sensitizer.

The value of the hole diffusion length (L_h) obtained from the fitting of the impedance spectrum is twice the thickness of the NiO cathode ($l = 2 \, \mu m$). Therefore, the efficient col-lection of photoinjected holes at the FTO/NiO interface is warranted since the average distance covered by the holes prior to any recombination/trapping event is longer than film thickness [62]. From equation (2), the relatively high value of L_h is mainly determined by the favorable combination of a low charge transport resistance ($R_t = 11 \, \Omega$, table 3), and comparatively high recombination resistance ($R_{rec.} = 45 \, \Omega$, table 3). The resulting diffusion coefficient calculated with equation (1) is thus remarkably high, with D_h in the order of $10^{-4} \, cm^2 \, s^{-1}$ (table 3) [12, 19]. Unlike the electrical behavior of a non-photoactive anode, this analysis proves that the elec-trical quality of the RDS NiO films here presented is also high when efficient dye-sensitizers are employed.

Conclusions

The optical and electrochemical properties of CoS as the anodic material of *p*-DSCs have been analyzed when the P1-sensitized NiO is the photoelectrochemically active cathode. The characterization of the *p*-DSCs with CoS anodes has been conducted in a comparative manner, taking the *p*-DSC with Pt-FTO as the term of comparison. The choice of CoS anode was motivated by the fact that CoS constitutes a cost-effective alternative to Pt-FTO. The photoelectrochem-ical cell with a CoS anode displayed a lower overall efficiency with respect to the device utilizing a Pt-FTO anode when the dye-sensitizer of the NiO photocathode was P1 (0.07 versus 0.11%). Such differences were ascribed to the limited capa-bility of CoS to sustain photocurrent densities larger than *ca.* 2 mA cm^{-2} for the slower kinetics of iodide oxidation at the CoS anode in comparison to the Pt-FTO counter electrode. The given upper threshold of photocurrent density is deter-mined by the dose of irradiation emitted by the sun simulator with AM1.5. On the basis of these differences, there was the 30 times larger charge transfer resistance of CoS with respect to Pt-FTO towards the oxidation of iodide (130 versus 4.5 Ω). The nature of the anodic material did not affect the values of open circuit potential (130 mV), the shape of the external quantum efficiency spectrum or the FF of the corresponding *p*-DSCs. On the basis of our previous experience it was also concluded that the FF was mainly controlled by the photo-conductive properties of the photoelectroactive cathode rather than the conductive properties of the counter electrode (i.e. the photoelectrochemically passive electrode). As a further step, it is suggested here that the CoS anodic films are prepared with a nanostructured morphology to increase the surface concen-tration of the electrochemically active sites. Another direction of research is the attainment of deposited CoS films with a larger extent of crystallinity. These additional characteristics are expected to diminish charge transfer resistance towards iodide oxidation and to improve the intrinsic charge transport

J. Phys. D: Appl. Phys. **50** (2017) 215501

M Bonomo *et al*

properties of optimized CoS. The modulation of CoS film thickness represents another direction of research for the optimization of the general performance of *p*-DSCs based on the improvement of the CoS anode.

Acknowledgments

References

[1] Grätzel M 2001 Photoelectrochemical cells *Nature* **414** 338–44

[2] Yella A, Lee H-W, Tsao H N, Yi C, Chandiran A K, Nazeeruddin M K, Diau E W-G, Yeh C-Y, Zakeeruddin S M and Gratzel M 2011 Porphyrin-sensitized solar cells with cobalt (II/III)-based redox electrolyte exceed 12 percent efficiency *Science* **334** 629

[3] Kakiage K, Aoyama Y, Yano T, Oya K, Fujisawa J and Hanaya M 2015 Highly-efficient dye-sensitized solar cells with collaborative sensitization by silyl-anchor and carboxy-anchor dyes *Chem. Commun.* **51** 15894–7

[4] Daeneke T, Kwon T-H, Holmes A B, Duffy N W, Bach U and Spiccia L 2011 High-efficiency dye-sensitized solar cells with ferrocene-based electrolytes *Nat. Chem.* **3** 213–7

[5] Mathew S, Yella A, Gao P, Humphry-Baker R, Curchod B F E, Ashari-Astani N, Tavernelli I, Rothlisberger U, Nazeeruddin M K and Grätzel M 2014 Dye-sensitized solar cells with 13% efficiency achieved through the molecular engineering of porphyrin sensitizers *Nat. Chem.* **6** 242

[6] Moser J E 2010 *Dye-Sensitized Solar Cells* ed K Kalyanasundaram (Lausanne: EPFL Press) pp 403–56

[7] Hagfeldt A and Graetzel M 1995 Light-induced redox reactions in nanocrystalline systems *Chem. Rev.* **95** 49–68

[8] Nattestad A, Ferguson M, Kerr R, Cheng Y-B and Bach U 2008 Dye-sensitized nickel (II) oxide photocathodes for tandem solar cell applications *Nanotechnology* **19** 295304

[9] Li M H, Yum J H, Moon S J and Chen P 2016 Inorganic p-type semiconductors: their applications and progress in dye-sensitized solar cells and perovskite solar cells *Energies* **9** 331

[10] Bonomo M and Dini D 2016 Nanostructured p-type semiconductor electrodes and photoelectrochemistry of their reduction processes *Energies* **9** 373

[11] Wood C J *et al* 2016 A comprehensive comparison of dye-sensitized NiO photocathodes for solar energy conversion *Phys. Chem. Chem. Phys.* **18** 10727

[12] Daeneke T *et al* 2015 Dominating energy losses in NiO p-type dye-sensitized solar cells *Adv. Energy Mater.* **5** 1401387

[13] Nattestad A, Mozer A J, Fischer M K R, Cheng Y-B, Mishra A, Bäuerle P and Bach U 2009 Highly efficient photocathodes for dye-sensitized tandem solar cells *Nat. Mater.* **9** 31–5

[14] Powar S *et al* 2013 Highly efficient p-type dye-sensitized solar cells based on tris(1,2-diaminoethane)cobalt(II)/(III) electrolytes *Angew. Chem., Int. Ed.* **52** 602–5

[15] Awais M, Dowling D D, Decker F and Dini D 2015 Photoelectrochemical properties of mesoporous NiO x deposited on technical FTO via nanopowder sintering in conventional and plasma atmospheres *Springerplus* **4** 564

[16] Tachiki M, Hosomi T and Kobayashi T 2000 Room-temperature heteroepitaxial growth of NiO thin films using pulsed laser deposition room-temperature heteroepitaxial growth of NiO thin films using pulsed laser deposition *Japan. J. Appl. Phys.* **39** 1817–20

[17] Bonomo M, Naponiello G, Di Carlo A and Dini D 2016 Characterization of screen-printed nickel oxide electrodes for p -type dye- sensitized solar cells *J. Mater. Sci. Nanotechnol.* **4** 201

[18] Awais M, Rahman M, Don MacElroy J M, Coburn N, Dini D, Vos J G and Dowling D P 2010 Deposition and characterization of NiO$_x$ coatings by magnetron sputtering for application in dye-sensitized solar cells *Surf. Coat. Technol.* **204** 2729–36

[19] Bonomo M, Barbero N, Matteocci F, Carlo A Di, Barolo C and Dini D 2016 Beneficial effect of electron-withdrawing groups on the sensitizing action of squaraines for p-type dye-sensitized solar cells *J. Phys. Chem.* C **120** 16340–53

[20] Gibson E A, Awais M, Dini D, Dowling D P, Pryce M T, Vos J G, Boschloo G and Hagfeldt A 2013 Dye sensitised solar cells with nickel oxide photocathodes prepared via scalable microwave sintering *Phys. Chem. Chem. Phys.* **15** 2411–20

[21] Rani A, Chung K, Kwon J, Kim S J, Jang Y H, Jang Y J, Quan L N, Yoon M, Park J H and Kim D H 2016 Layer-by-layer self-assembled graphene multilayers as pt-free alternative counter electrodes in dye-sensitized solar cells *ACS Appl. Mater. Interfaces* **8** 11488–98

[22] Jin J, Zhang X and He T 2014 Self-Assembled CoS$_2$ nanocrystal film as an efficient counter electrode for dye-sensitized solar cells *J. Phys. Chem.* C **118** 24877–83

[23] Kung C W, Chen H W, Lin C Y, Huang K C, Vittal R and Ho K C 2012 CoS acicular nanorod arrays for the counter electrode of an efficient dye-sensitized solar cell *ACS Nano* **6** 7016–25

[24] Yao R Y, Zhou Z J, Hou Z L, Wang X, Zhou W H and Wu S X 2013 Surfactant-free CuInS$_2$ nanocrystals: an alternative counter-electrode material for dye-sensitized solar cells *ACS Appl. Mater. Interfaces* **5** 3143–8

[25] Yang D S, Kim C, Song M Y, Park H Y, Kim J C, Lee J J, Ju M J and Yu J S 2014 N-doped hierarchical hollow mesoporous carbon as metal-free cathode for dye-sensitized solar cells *J. Phys. Chem.* C **118** 16694–702

[26] Roy-Mayhew J D and Aksay I A 2014 Graphene materials and their use in dye-sensitized solar cells *Chem. Rev.* **114** 6323–48

[27] Gong F, Wang H, Xu X, Zhou G and Wang Z S 2012 *In situ* growth of Co(0.85)Se and Ni(0.85)Se on conductive substrates as high-performance counter electrodes for dye-sensitized solar cells *J. Am. Chem. Soc.* **134** 10953–8

[28] Wu M, Lin X, Wang Y, Wang L, Guo W, Qi D, Peng X, Hagfeldt A, Grätzel M and Ma T 2012 Economical Pt-free catalysts for counter electrodes of dye-sensitized solar cells *J. Am. Chem. Soc.* **134** 3419–28

[29] Wu M and Ma T 2014 Recent progress of counter electrode catalysts in dye-sensitized solar cells *J. Phys. Chem.* C **118** 16727–42

[30] Li L, Yang Y, Fan R, Chen S, Wang P, Yang B and Cao W 2014 Conductive upconversion Er,Yb-FTO nanoparticle coating to replace Pt as a low-cost and high-performance counter electrode for dye-sensitized solar cells *ACS Appl. Mater. Interfaces* **6** 8223–9

[31] Congiu M, Bonomo M, De Marco M L, Dowling D P, Di Carlo A, Dini D and Graeff C F O 2016 Cobalt sulfide as

J. Phys. D: Appl. Phys. 50 (2017) 215501

M Bonomo *et al*

counter electrode in p-type dye-sensitized solar cells *Chem. Select* **1** 2808–15

[32] Tai S Y, Chang C F, Liu W C, Liao J H and Lin J Y 2013 Optically transparent counter electrode for dye-sensitized solar cells based on cobalt sulfide nanosheet arrays *Electrochim. Acta* **107** 66–70

[33] Wang G and Zhuo S 2013 Hierarchical micro/nano-structured cobalt sulfide spindles as low-cost counter electrodes for dye-sensitized solar cells *Phys. Chem. Chem. Phys.* **15** 13801

[34] Mulmudi H K, Batabyal S K, Rao M, Prabhakar R R, Mathews N, Lam Y M and Mhaisalkar S G 2011 Solution processed transition metal sulfides: application as counter electrodes in dye sensitized solar cells (DSCs) *Phys. Chem. Chem. Phys.* **13** 19307–9

[35] Hao F, Dong P, Luo Q, Li J, Lou J and Lin H 2013 Recent advances in alternative cathode materials for iodine-free dye-sensitized solar cells *Energy Environ. Sci.* **6** 2003

[36] Lin J-Y, Tsai Y-T, Tai S-Y, Lin Y-T, Wan C-C, Tung Y-L and Wu Y-S 2012 Pulse-reversal deposition of cobalt sulfide thin film as a counter electrode for dye-sensitized solar cells *J. Electrochem. Soc.* **160** D46–52

[37] Zampetti A, De Rossi F, Brunetti F, Reale A, Di Carlo A and Brown T M 2014 Electrodeposited cobalt sulfide hole collecting layer for polymer solar cells *Appl. Phys. Lett.* **105** 063304

[38] De Rossi F, Di Gaspare L, Reale A, Di Carlo A and Brown T M 2013 Blending CoS and Pt for amelioration of electrodeposited transparent counterelectrodes and the efficiency of back-illuminated dye solar cells *J. Mater. Chem.* A **1** 12941

[39] Wang M, Anghel A M, Marsan B, Ha N L C, Pootrakulchote N, Zakeeruddin S M and Grätzel M 2009 CoS supersedes Pt as efficient electrocatalyst for triiodide reduction in dye-sensitized solar cells *J. Am. Chem. Soc.* **131** 15976–7

[40] Qin P, Zhu H, Edvinsson T, Boschloo G, Hagfeldt A and Sun L 2008 Design of an organic chromophore for P-type dye-sensitized solar cells *J. Am. Chem. Soc.* **130** 8570

[41] Wood C J, Summers G H and Gibson E A 2015 Increased photocurrent in a tandem dye-sensitized solar cell by modifications in push–pull dye-design *Chem. Commun.* **51** 3915

[42] Wood C J *et al* 2014 Red-absorbing cationic acceptor dyes for photocathodes in tandem solar cells *J. Phys. Chem.* C **118** 16536–46

[43] Wood C J, Robson K C D, Elliott P I P, Berlinguette C P and Gibson E A 2014 Novel triphenylamine-modified ruthenium(ii) terpyridine complexes for nickel oxide-based cathodic dye-sensitized solar cells *RSC Adv.* **4** 5782–91

[44] Wild M, Griebel J, Hajduk A, Friedrich D, Stark A, Abel B and Siefermann K R 2016 Efficient synthesis of triarylamine-based dyes for p-type dye-sensitized solar cells *Sci. Rep.* **6** 1–8

[45] Congiu M, Decker F, Dini D and Graeff C F O 2016 An open-source equipment for thin film fabrication by electrodeposition, dip coating, and SILAR *Int. J. Adv. Manuf. Technol.* 1–9

[46] Dini D, Decker F and Masetti E 1996 A comparison of the electrochromic properties of WO_3 films intercalated with H+, Li+ and Na+ *J. Appl. Electrochem.* **26** 647

[47] Srinivasa Rao S, Gopi C V V M, Kim S K, Son M K, Jeong M S, Savariraj A D, Prabakar K and Kim H J 2014 Cobalt sulfide thin film as an efficient counter electrode for dye-sensitized solar cells *Electrochim. Acta* **133** 174–9

[48] Sheehan S, Naponiello G, Odobel F, Dowling D P, Di Carlo A and Dini D 2015 Comparison of the photoelectrochemical properties of RDS NiO thin films for p-type DSCs with different organic and organometallic dye-sensitizers and evidence of a direct correlation between cell efficiency and charge recombination *J. Solid State Electrochem.* **19** 975–86

[49] Boschloo G and Hagfeldt A 2009 Characteristics of the iodide/triiodide redox mediator in dye-sensitized solar cells *Acc. Chem. Res.* **42** 1819–26

[50] Bard A J and Faulkner L R 2001 *Electrochemical Methods, Fundamentals and Applications* 2nd edn (New York: Wiley) pp 156–260

[51] Petrocco A, Liberatore M, Di Carlo A, Reale A, Brown T M and Decker F 2010 Thermal activation of mass transport and charge transfer at Pt in the I_3^-/I^- electrolyte of a dye-sensitized solar cell *Phys. Chem. Chem. Phys.* **12** 10786–92

[52] He J, Lindström H, Hagfeldt A and Lindquist S-E 2000 Dye-sensitized nanostructured tandem cell-first demonstrated cell with a dye-sensitized photocathode *Sol. Energy Mater. Sol. Cells* **62** 265

[53] Bonomo M, Naponiello G, Venditti I, Zardetto V, Carlo A Di and Dini D 2017 Electrochemical and photoelectrochemical properties of screen-printed nickel oxide thin films obtained from precursor pastes with different compositions *J. Electrochem. Soc.* **164** H137–47

[54] Pitarch Á, Garcia-Belmonte G, Mora-Seró I and Bisquert J 2004 Electrochemical impedance spectra for the complete equivalent circuit of diffusion and reaction under steady-state recombination current *Phys. Chem. Chem. Phys.* **6** 2983–8

[55] Awais M, Dowling D P, Decker F and Dini D 2015 Electrochemical characterization of nanoporous nickel oxide thin films spray-deposited onto indium-doped tin oxide for solar conversion scopes *Adv. Condens. Matter Phys.* **2015** 186375

[56] Novelli V, Awais M, Dowling D P and Dini D 2015 Electrochemical characterization of rapid discharge sintering (RDS) NiO cathodes for dye-sensitized solar cells of p-type *Am. J. Anal. Chem.* **6** 176–87

[57] Naponiello G, Venditti I, Zardetto V, Saccone D, Di Carlo A, Fratoddi I, Barolo C and Dini D 2015 Photoelectrochemical characterization of squaraine-sensitized nickel oxide cathodes deposited via screen-printing for p-type dye-sensitized solar cells *Appl. Surf. Sci.* **356** 911–20

[58] Awais M, Gibson E, Vos J G, Dowling D P, Hagfeldt A and Dini D 2014 Fabrication of efficient NiO photocathodes prepared via RDS with novel routes of substrate processing for p-type dye-sensitized solar cells *Chem. Electron. Chem.* **1** 384

[59] Awais M, Dowling D D, Rahman M, Vos J G, Decker F and Dini D 2013 Spray-deposited NiO_x films on ITO substrates as photoactive electrodes for p-type dye-sensitized solar cells *J. Appl. Electrochem.* **43** 191–7

[60] Awais M, Rahman M, Don MacElroy J M, Dini D, Vos J G and Dowling D P 2011 Application of a novel microwave plasma treatment for the sintering of nickel oxide coatings for use in dye-sensitized solar cells *Surf. Coat. Technol.* **205** S245–9

[61] Fabregat-Santiago F, Bisquert J, Palomares E, Otero L, Kuang D, Zakeeruddin S M and Grätzel M 2007 Correlation between photovoltaic performance and impedance spectroscopy of dye-sensitized solar cells based on ionic liquids *J. Phys. Chem.* C **111** 6550–60

[62] Peter L M and Wijayantha U K G 1999 Intensity dependence of the electron diffusion length in dye-sensitised nanocrystalline TiO_2 photovoltaic cells *Electrochem. Commun.* **1** 576